ELSEVIER

Journal of Structural Geology 26 (2004) 869–883

JOURNAL OF STRUCTURAL GEOLOGY

www.elsevier.com/locate/jsg

Development of single-crystal σ-shaped quartz porphyroclasts by dissolution–precipitation creep in a calcite marble shear zone

Michel Bestmann[a,*], David J. Prior[a], Kees T.A. Veltkamp[b]

[a]*Department of Earth Sciences, Liverpool University, Liverpool L69 3GP, UK*
[b]*School of Biological Sciences, Liverpool University, Liverpool L69 3GP, UK*

Received 30 January 2003; received in revised form 16 October 2003; accepted 20 October 2003

Abstract

Within a greenschist facies calcite marble shear zone, isolated quartz grains change shape across the shear zone profile. Whereas quartz grains have a spherical to elongated shape in the coarse grained marble protolith and protomylonite, they are asymmetric σ-shaped porphyroclasts with wedge shaped appendages (wings) in ultramylonites. In all cases quartz grains are single-crystals. They are sometimes twinned but never recrystallized. Stress-induced dissolution–precipitation creep is the favourable shape-controlling process during deformation providing a relatively undeformed core, truncation of pre-existing cathodoluminescence (CL) patterns and syntaxial precipitation of wings. The necessary fluids may have been released from fluid inclusions during dynamic recrystallization of the calcite matrix. The development of σ-shape is not related to the crystallographic orientation of the quartz porphyroclasts. Crystallographic orientation analysis by electron backscatter diffraction (EBSD) and CL analyses exclude crystal-plasticity as a shape-controlling mechanism of quartz grains during mylonitisation. However, in ultramylonites quartz clasts have a strong crystallographic preferred orientation (CPO), with *c*-axes (sub)parallel to the shear direction. This fabric is uncommon for quartz under greenschist facies conditions. It might be explained by a strengthening of a pre-existing weak CPO during mylonitisation by rigid particle rotation of elongated quartz grains.

Keywords: Quartz; σ-Shape; Porphyroclast; Dissolution–precipitation creep; Calcite marble; Electron backscatter diffraction (EBSD); Cathodoluminescence

1. Introduction

Many mylonites contain porphyroclasts embedded as relatively rigid inclusions in a fine-grained, ductile matrix. The porphyroclasts occur in a wide range of sizes and shape geometries and are important shear sense indicators (e.g. Passchier and Simpson, 1986). The strain-induced shape of porphyroclasts depends on the geometry of flow lines of the viscous matrix around and its interaction with the rigid particle (e.g. Passchier and Sokoutis, 1993; Pennacchioni et al., 2001; Mancktelow et al., 2002). The degree of bonding between matrix and inclusion has an especially strong effect on the flow-induced differential stress distribution in the clasts and therefore on the shape controlling deformation mechanism (Kenkmann, 2000). Mantled porphyroclasts, consisting of a porphyroclast core and a mantle/wings of recrystallized material with σ-shape geometry develop during non-coaxial flow (Tullis and Yund, 1985; Passchier and Simpson, 1986; Dell'Angelo and Tullis, 1989). σ-Type shapes have also been reported for single-crystal porphyroclasts. These single-crystals exist for a variety of mineral phases, for example, of mica, K-feldspar, tourmaline, hypersthene, quartz (ten Grotenhuis et al., 2003), hornblende, olivine (Mancktelow et al., 2002), garnet (Azor et al., 1997; ten Grotenhuis et al., 2003), and sillimanite (Pennacchioni et al., 2001).

Because of its importance in nature the deformation behaviour of quartz in different rheological environments is a particular point of interest. However, quartz porphyroclasts are uncommon in mylonitic rocks, since quartz tends to constitute the matrix rather than porphyroclasts in most mylonites. Quartz can only survive as porphyroclasts in a soft and usually fine-grained matrix. ten Grotenhuis et al. (2003) reported from a lower greenschist facies protomylonite of volcanic origin that fish-shaped quartz porphyroclasts were formed by crystal-plastic deformation. We

* Corresponding author. Present address: Department of Geological Sciences, University of Vienna, Althanstrasse 14, A-1090 Vienna, Austria. Tel.: +43-1-427753471; fax: +43-1-42779534.
E-mail address: michel.bestmann@univie.ac.at (M. Bestmann).

0191-8141/$ - see front matter © 2004 Elsevier Ltd. All rights reserved.
doi:10.1016/j.jsg.2003.10.003

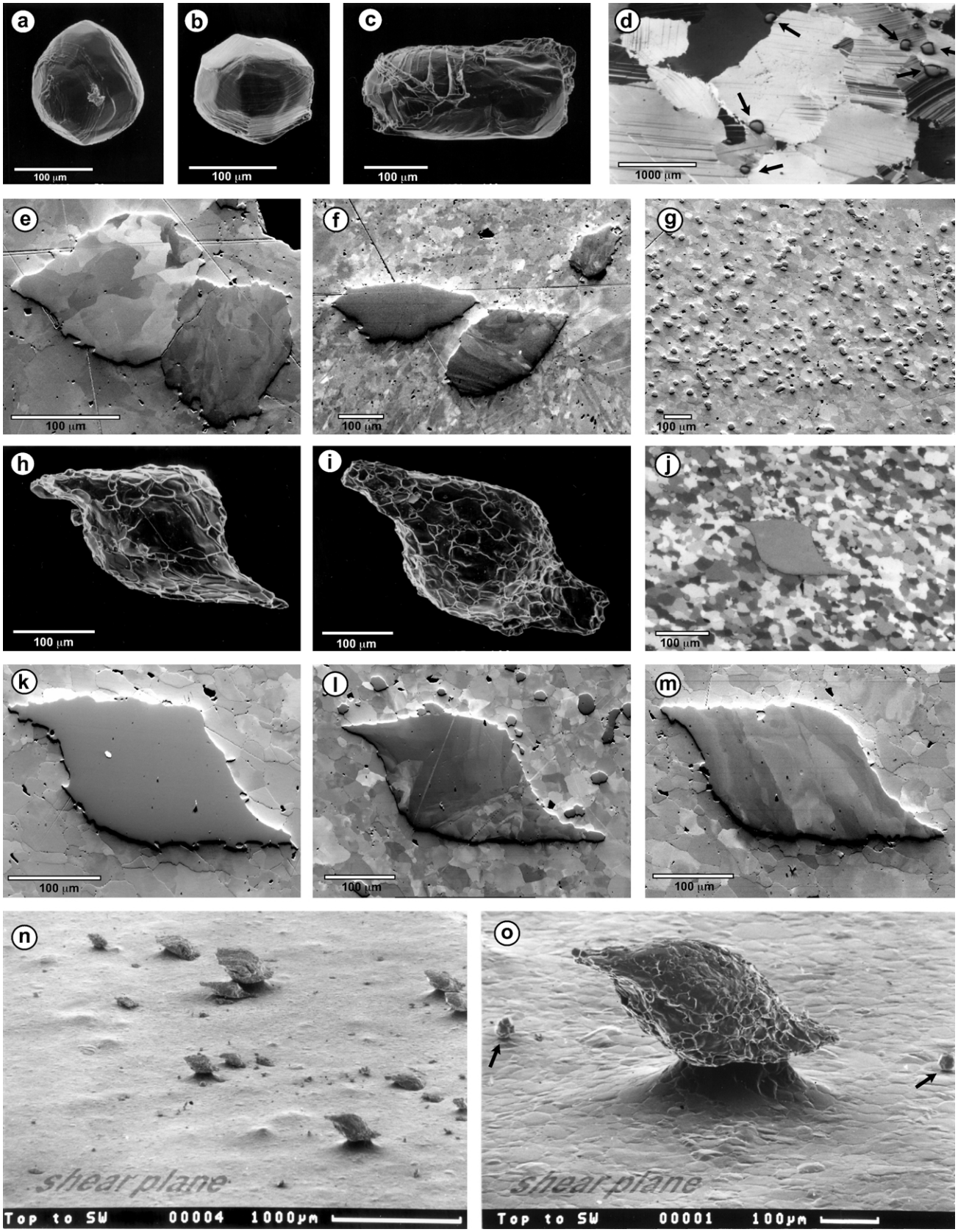

Fig. 1. (a)–(f) Quartz grains in the coarse-grained protolith and protomylonite marble. (a)–(c) SEM photographs of quartz grains with different three-dimensional shape extracted by acid etching (Bestmann, 2000). (d) Microphotographs (reflected light) of the position of quartz grains (showing positive relief; see also arrows) within the calcite microstructure. (e) and (f) SEM-OC (orientation contrast) images of quartz grains in the protomylonite marble. Quartz grains

present a study of quartz grains embedded within a marble shear zone on Thassos Island, Greece. In contrast to the quartz porphyroclasts described by ten Grotenhuis et al. (2003) with recrystallized grains in the tips, the σ-shaped quartz grains embedded in the calcite ultramylonite are single-crystals (Bestmann, 2000). Since the evolution of the greenschist facies marble shear zone is well constrained (Bestmann et al., 2000) the question still remains whether these clasts were formed by crystal plasticity (dislocation creep) or diffusional processes (i.e. dissolution–precipitation creep). To verify what mechanism leads to the σ-shape optical microscopy, electron backscatter diffraction (EBSD) technique and cathodoluminescence (CL) analysis in a scanning electron microscope (SEM) were applied.

2. Methods

2.1. Sample preparation

Thin sections and polished blocks from different positions of the shear zone profile were made parallel to the shear direction and perpendicular to the shear zone boundary (*xy*-plane). The shear direction was deduced from the geometry of the σ-shaped quartz grains extracted by in-situ etching from the calcite matrix of the ultramylonite (Bestmann, 2000). Sample chips were SYTON-polished for EBSD-SEM and CL-SEM studies (Fynn and Powell, 1979; Lloyd, 1987; Prior et al., 1996).

2.2. EBSD analysis

Full crystallographic orientation data were obtained from automatically indexed EBSD patterns collected in a CamScan X500 crystal probe fitted with a thermionic field emission gun and a FASTRACK stage. Working conditions were: 20 kV acceleration voltage, 20 nA beam current and 25 mm working distance. The stored EBSD patterns were indexed by using the program CHANNEL 5.03 from HKL software. The centre of seven Kikuchi bands was automatically detected using the Hough transform routine (Adams et al., 1993) with a resolution of 100 (internal Hough resolution parameter in the software). The solid angles calculated from the patterns were compared with a quartz and calcite match unit containing 75 reflectors to index the patterns.

Data about crystallographic preferred orientation (CPO) were constrained by measuring the orientation of individual quartz grains within a set of protolith/protomylonite and ultramylonite samples; one orientation measurement per grain. Several quartz grains were mapped by automatic scans (beam and stage scan) on a square grid with a fixed step size of 1 or 2 μm. All EBSD patterns that could not be indexed were stored. These EBSD patterns were used to perform offline reanalyses to improve the orientation maps. Instead of the initial setting of seven automatically detected Kikuchi bands, six bands and, subsequently, five bands were used. This enhances the probability, for the acquisition software to find a solution. The reliability of the results was checked by comparing the reanalysed orientations with the neighbour orientations. This procedure allowed the total amount of non-indexed points to be reduced from initially ~15% down to ~3%.

2.3. SEM cathodoluminescence (CL) and backscattered (BSE) analysis

CL and BSE studies were carried out by a Philips XL30 SEM fitted with a K.E. Developments Ltd cathodoluminescence detector (D308122). Working conditions were: 10 kV (15 kV for BSE) acceleration voltage, 10 nA beam current and 16 mm working distance. CL images were obtained by accumulating the signal of 16 frames using a slow scanning beam raster.

3. Geology and shear zone characterization

The poly-metamorphic complex of Thassos Island, Greece, is dominated by massive marble units with intercalations of paragneisses and orthogneisses. The rocks show fabric development under retrograde metamorphic conditions (Peterek et al., 1994; Wawrzenitz and Krohe, 1998). Maximum metamorphic conditions during Alpine tectonics (Dinter, 1998) were between 580 °C/2.4 kbar and 620 °C/4.7 kbar (Bestmann et al., 2000). During extensional tectonics, linked to the exhumation of the metamorphic core complex, strain partitioning occurred during decreasing pressure–temperature conditions. Within the pure calcite marbles, this stage of deformation is recorded by several shear zones, up to 3 m in thickness, which are oriented parallel to the host rock foliation plane.

show different lattice distortion patterns. (g) SEM-OC image of small quartz grains enriched in a horizon of the ultramylonite marble. (h)–(o) Asymmetrical quartz grains (σ-shaped) with stair-stepping appendages (wings) in the ultramylonite marble. (h) and (i) SEM-photographs of a quartz grain extracted by acid etching photographed from two different perspectives. The surface network reflects the relief of the dissolved calcite fabric at the interface to the ultramylonite matrix (grain boundary network). (j) Microphotograph (reflected light) of σ-shaped quartz grain and surrounding calcite ultramylonite matrix (*xz*-section). (k)–(m) SEM-OC images of σ-shaped quartz grains with different internal lattice distortion patterns (*xz*-section). At the quartz–calcite interface quartz penetrates into the adjacent calcite–calcite grain boundary network (best seen in (k)) and produced the surface network seen in (h) and (i). (n) and (o) SEM-photographs of σ-shaped quartz grains situated in-situ on the shear plane of the calcite ultramylonite. All grains have the same σ-shaped orientation with respect to the shear plane. The geometry of the quartz grains indicates a dominant non-coaxial deformation of the ultramylonite marble, with shear direction of the hanging wall toward the SW. Arrows in (o) mark small quartz grains, which do not show the characteristic σ-shape.

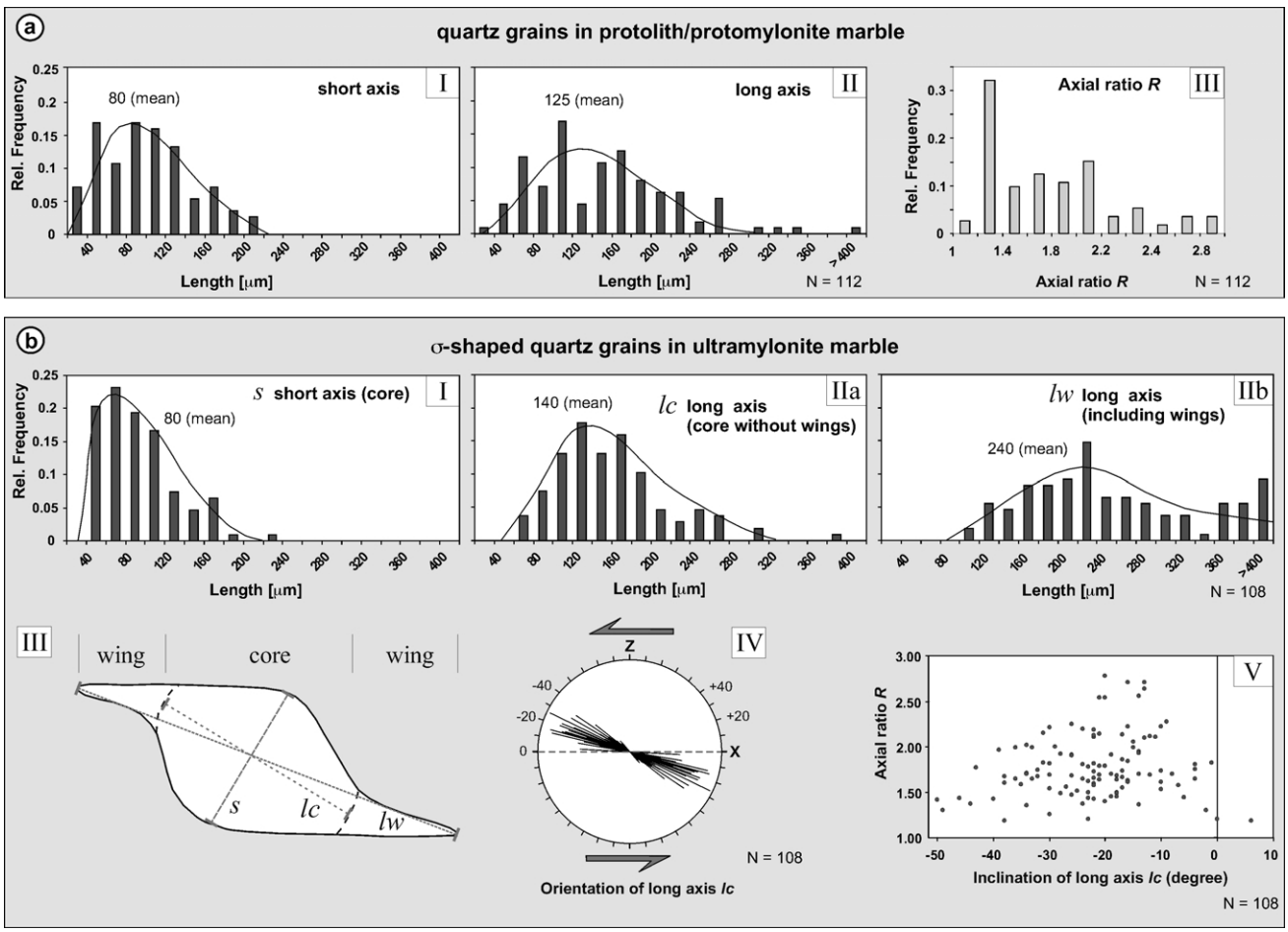

Fig. 2. Grain parameter of (a) quartz grains in the protolith/protomylonite and (b) σ-shaped quartz grains in the ultramylonite marble. (a) The length of the short (I) and the long axis (II) and the axial ratio *R* (III) is given. (b) For the σ-shaped clasts two different long axes are presented (see sketch III): (IIa) maximum length of the core of the grain without the wings (*lc*) and (IIb) the total length of the quartz grains including wings (*lw*). General trend line and mean values are given. (III) Sketch showing the measured grain parameters of σ-shaped quartz grains. (IV) Orientation of long axes *lc* with respect to the shear plane (dashed line). Note the antithetic angle with respect to the given shear sense. (V) Axial ratio *R* versus orientation of *lc*.

The sample location for this study is given in Bestmann et al. (2000). The coarse-grained (grain size 1–3 mm) marble protolith outside shear zones is characterized by symmetrically oriented twin sets and by nearly orthorhombic symmetry of calcite CPO due to early coaxial deformation (Bestmann et al., 2000). Fluid inclusions within the coarse calcite grains are common (Bestmann, 2000). The shear zone boundaries (SZB) are marked by sharp transitions in the grain size, through a narrow zone of protomylonitic fabric. The fine-grained ultramylonite (grain size 10–30 μm) has a generally homogeneous microstructure. In ultramylonites, the mylonitic foliation is oriented parallel to the shear zone boundary (SZB) and reflects the shear plane. Within the shear zone a dominant component of non-coaxial deformation is indicated by the shape-preferred orientation of the calcite grains in the matrix, oblique to the SZB, and by the asymmetric shape of the quartz porphyroclasts (Bestmann et al., 2000). Stable isotope analysis constrained by Bestmann (2000) provided no evidence for the influx of external fluids into the shear zone.

4. Microfabrics of the quartz grains

In general, quartz grains comprise less than 1% volume of the calcite marble. Some horizons can be enriched in quartz grains. However, the quartz grains are mostly single-crystals isolated within the calcite matrix.

4.1. Quartz grains in the protolith and protomylonite marble

Within the coarse-grained marble protolith and protomylonite, quartz grains (grain size range 10–300 μm) occur inside the calcite grains or at their grain boundaries (Fig. 1d). SEM images of individual grains, extracted by etching (Bestmann, 2000), reveal spherical (Fig. 1a), sometimes facetted (Fig. 1b) to elongated (Fig. 1c) shapes. The axial ratio, *R*, ranges between 1 and 3 (mean 1.5) (Fig. 2a). Most of the quartz grains exhibit undulose extinction under the transmitted light microscope. SEM orientation contrast (OC) images indicate small orientation domains within individual grains (Fig. 1e

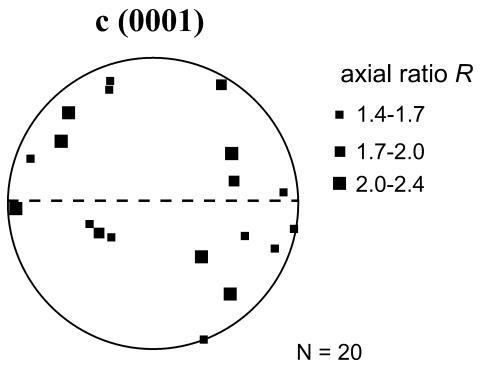

Fig. 3. *C*-axis plot of elongated quartz grains extracted (by etching) from the protolith/protomylonite marble. *C*-axes are presented with respect to the orientation of grain long axes (horizontal dashed line). Only quartz grains with an axial ration of $R > 1.4$ were measured. Range of axial ratio is indicated (see key).

and f). EBSD measurements of elongated quartz grains extracted from the protolith/protomylonite marble reveal that the *c*-axes can scatter with a relatively high angle with respect to the long axis of elongated grains (Fig. 3). The data do not show any correlation between axial ratio and *c*-axis orientation.

The orientation maps (Fig. 4a and b) reveal that distinct parts of the quartz grains are separated by Dauphiné twin boundaries. Dauphiné twinning involves a 180° (or apparent 60°) rotation about the quartz *c*(0001) axis. Thus, there is no effect on the orientations of the *c*(0001), *m*{10$\bar{1}$0} or *a*⟨11$\bar{2}$0⟩ directions, although $+a$ and $-a$ are interchanged and *r*{10$\bar{1}$1} and *z*{01$\bar{1}$1} are interchanged. Most neighbouring domains visible in the OC image have boundaries with less than 2° misorientation.

Dispersion patterns in the pole figures reveal intracrystalline lattice distortion (Fig. 5). Plots of misorientation axes indicate lattice rotation mainly around the crystallographic *c*-axis, and to a minor extent around the pole of the π-plane {10$\bar{1}$2}, *r*-plane {10$\bar{1}$1} or ξ-plane {11$\bar{2}$2} (Fig. 5). Even though a misorientation axis of low misorientation angle can contain a significant error (Prior, 1999), Bestmann and Prior (2003) showed that a statistically representative data set is able to give reliable average misorientation axes for angles less than 10°.

The quartz grains within the protolith/protomylonite show a weak crystallographic preferred orientation (Fig. 7a) even though the number of measured grains is relatively small. The *c*-axes build a weak girdle distribution parallel to the *xy* reference plane.

Quartz grains display various SEM-CL features within different parts of the grains (invisible in BSE or in the OC images) resulting as shades of grey, ranging from black (weak or no SEM-CL) to light grey (strong SEM-CL) (Fig. 8a–d). Many grains contain concentric zones (5–30 μm wide) around a core revealed by gradual to sharp transition in SEM-CL intensity. Some CL zones, i.e. the cores of the quartz grains, are facetted (Fig. 8a and d). There is no general trend in the grey level shade (i.e. from dark to bright) from the core towards the margin of the quartz grains. Less commonly, quartz grains display nearly uniform luminescence across the grain (Fig. 8c). Some grains display a diffuse network of bright SEM-CL pattern (Fig. 8b). The quartz grains display a discontinuous thin black rind (1–2 μm in thickness) at the interface with the calcite matrix. In general there is no specific difference in the SEM-CL patterns between quartz grains from the protolith and quartz grains from the protomylonite, even if the latter might develop structures that look like symmetric wedge-shaped wings (Fig. 8b and d).

4.2. Quartz grains in the ultramylonite marble

Quartz grains embedded in the fine-grained calcite matrix have a monoclinic shape symmetry comparable with that of σ-type porphyroclast systems (Passchier and Simpson, 1986) except that they are generally single-crystals and do not include recrystallized material (Fig. 1h–o). All σ-shaped quartz grains have the same shape asymmetry and geometric orientation reflecting the sense of shear (Fig. 1n). The network on the quartz surface (Fig. 1h, i and o) reflects calcite–quartz–calcite triple junctions and shows the remaining grain boundary network of the dissolved calcite microstructure at the interface between quartz and ultramylonitic matrix. In sections this microstructure is characterised by marginal quartz spikes intruding into adjacent calcite boundaries (e.g. Figs. 1k and 8h).

The size of the core of the asymmetrical quartz grains (*lc*) varies between 50 and 300 μm with an axial ratio of $R = 1.2–2.8$ (mean 1.7) (Fig. 2b). The long axes of the core (*lc*) are inclined at an antithetic angle $<50°$ to the shear plane. There is a weak *R*-dependence with respect to a main inclination angle *lc* of 10–30° for grains with $R > 2$. The maximum length of the grains including the wings (*lw*) varies between 100 and 600 μm. Therefore the distribution of long axes from the protolith/protomylonite quartz grains (Fig. 2a) is in the same range as *lc*. In contrast, *lw* reaches higher values than the long axis of grains in the protolith/protomylonite.

In transmitted light the 'σ-shaped' quartz grains show generally uniform extinction. Where undulose extinction is observed it sweeps through the whole grain rather than being restricted to the wings. In the SEM the σ-shaped quartz grains show a variety of internal OC patterns (Fig. 1k–m). Many of the quartz grains are homogeneous without any variation of the orientation contrast (Fig. 1k), some contain a mosaic of small oblique (with respect to the shear plane) OC domains (Fig. 1m) and others show heterogeneous OC patterns (Fig. 1l).

The orientation maps (Fig. 4c–e) reveal that in general the OC domains have boundaries with less than 2° misorientation. Dauphiné twin boundaries separate distinct areas within the grains but are not related to specific parts of the quartz grains.

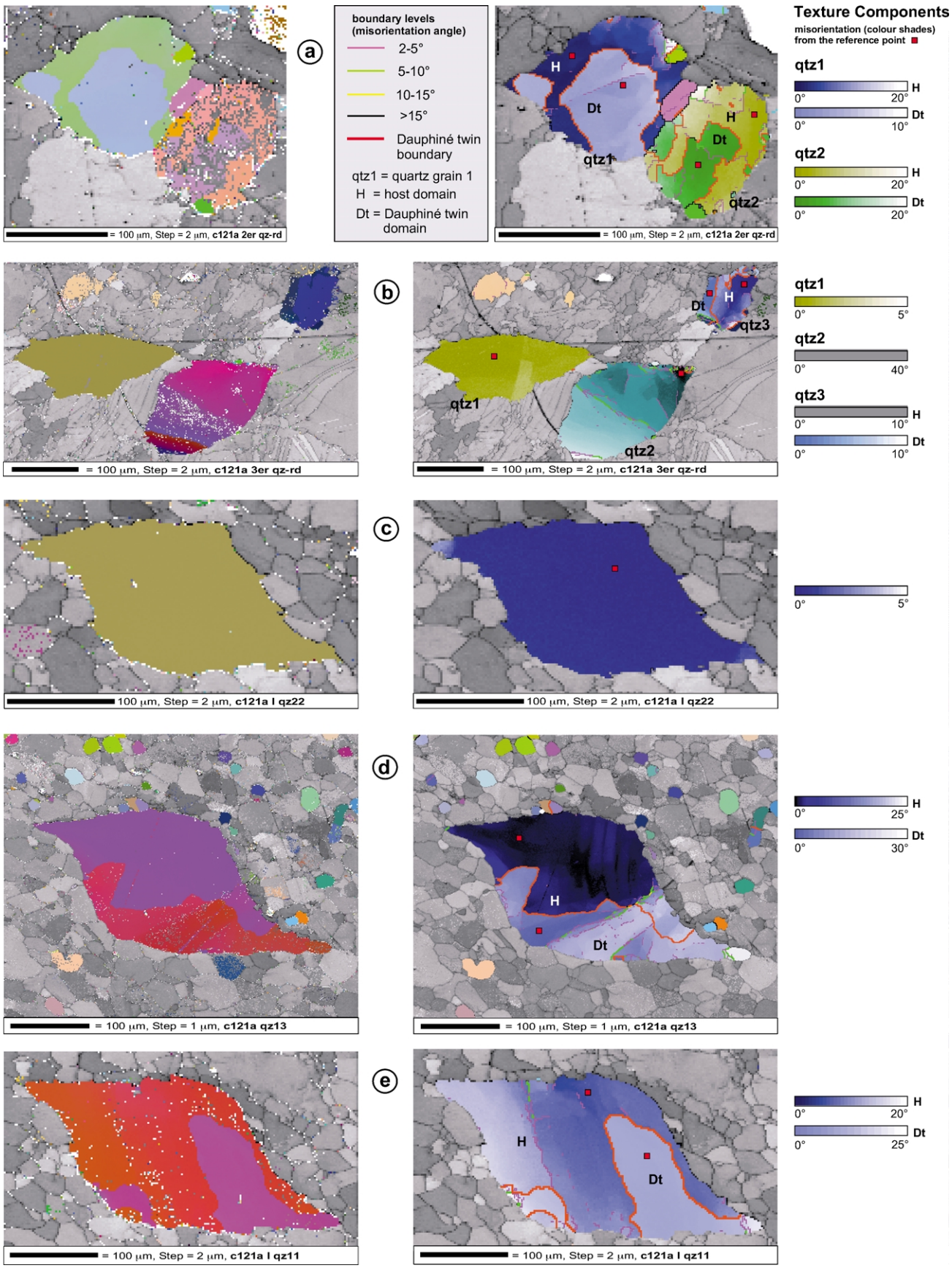
a
boundary levels (misorientation angle)
2-5°
5-10°
10-15°
>15°
Dauphiné twin boundary
qtz1 = quartz grain 1
H = host domain
Dt = Dauphiné twin domain
H
Dt
qtz1
qtz2
= 100 µm, Step = 2 µm, c121a 2er qz-rd
Texture Components
misorientation (colour shades) from the reference point
qtz1
H 0° 20°
Dt 0° 10°
qtz2
H 0° 20°
Dt 0° 20°
b
qtz3
= 100 µm, Step = 2 µm, c121a 3er qz-rd
qtz1 0° 5°
qtz2 0° 40°
qtz3
H 0° 10°
Dt 0° 10°
c
= 100 µm, Step = 2 µm, c121a l qz22
0° 5°
d
= 100 µm, Step = 1 µm, c121a qz13
H 0° 25°
Dt 0° 30°
e
= 100 µm, Step = 2 µm, c121a l qz11
H 0° 20°
Dt 0° 25°

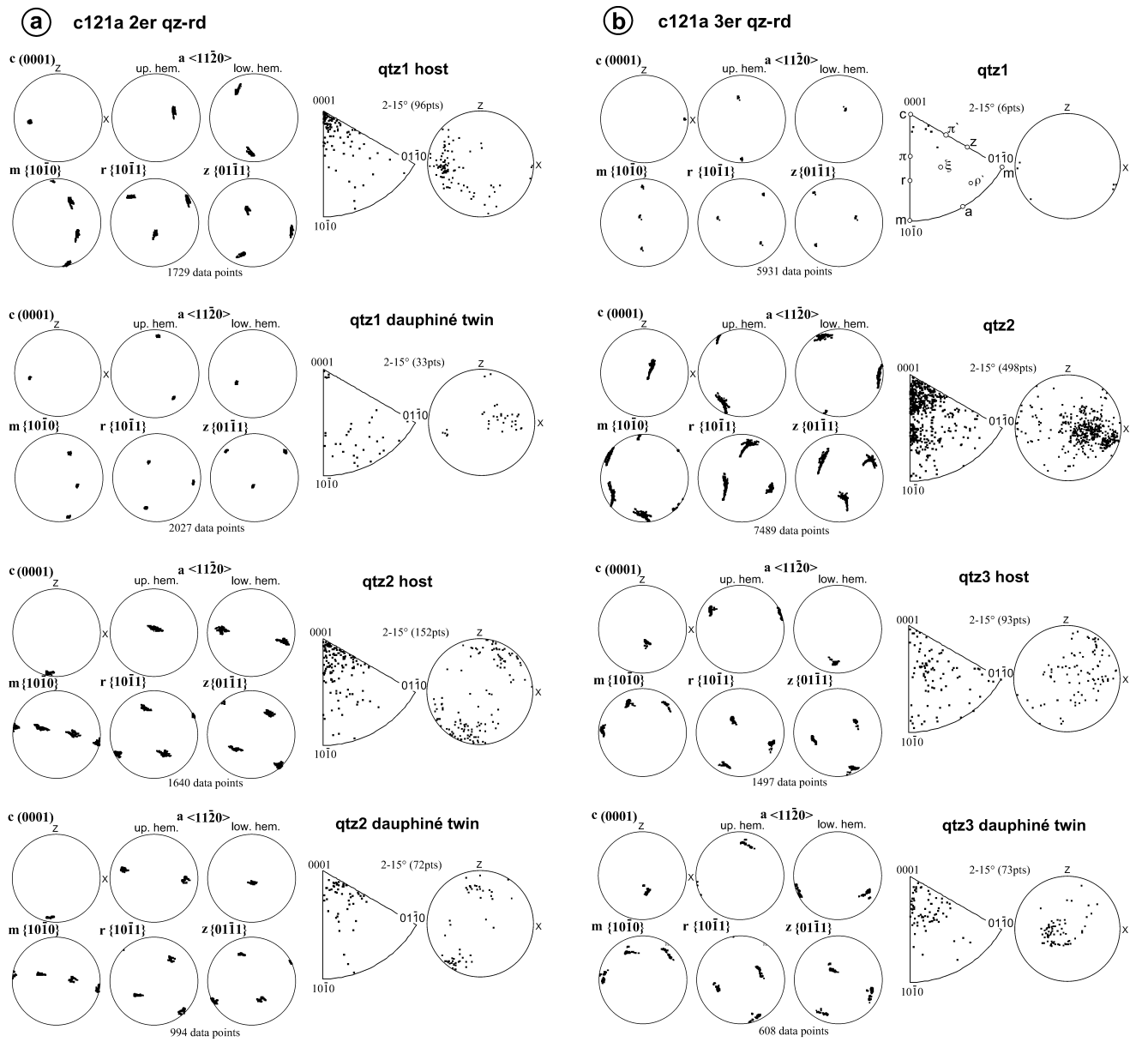

Fig. 5. Orientation and misorientation data from the analysed quartz grains in the protolith/protomylonite marble (Fig. 4): (a) scan C121a 2er qz-rd (see Fig. 4a); (b) scan c121a 3er qz-rd (see Fig. 4b). Host and Dauphiné twin domains are presented separately. The crystallographic orientation data of the individual quartz grain domains are plotted as pole figures. Six pole figures on the left of each data set are equal area upper hemisphere stereoplots. To distinguish between the two different crystallographic *a*-axes in quartz, $+a$- and $-a$-axis, these are plotted in both hemispheres. Dispersion patterns in pole figures reveal lattice distortion. The distribution of misorientation axes for low angle misorientations (2–15°) is presented, on the right, with respect to the crystal reference frame (IPF: equal angle, upper hemisphere projection) and with respect to the sample reference frame (stereoplot: equal area, upper hemisphere projection). For each plot the number of data points (pts) is given.

Fig. 4. EBSD maps of quartz grains from (a) and (b) the protomylonite marble and (c)–(e) the ultramylonite marble. The orientation maps correspond to the microstructures presented as SEM-OC images in Fig. 1e, f and k–m, respectively. Left maps are constructed from the raw EBSD data. The orientation of quartz is displayed by different colours (related to the three Euler angles), whereas the microstructure of calcite is represented by grey shades (EBSD pattern quality). Some of the EBSD patterns were indexed as the wrong phase because both calcite and quartz have trigonal crystal symmetry. Data are on a grid with 1 or 2 μm spacing (see individual maps). Right maps are processed to remove erroneous data and non-indexed points (white points in left maps) (for details see Prior et al., 2002). To show gradual lattice distortion within the quartz grains the orientation of individual quartz grains is colour shaded as texture components (see also Bestmann and Prior, 2003) according to their angular misorientation (for definition see Wheeler et al., 2001) from the points marked by red squares in the host and Dauphiné twin domains, respectively. The dominant orientation domain within a quartz grain was defined as the host domain, the minor one as the Dauphiné twin domain. Boundaries related to different misorientation intervals are presented as coloured lines (see key). The Dauphiné twin boundary is marked separately.

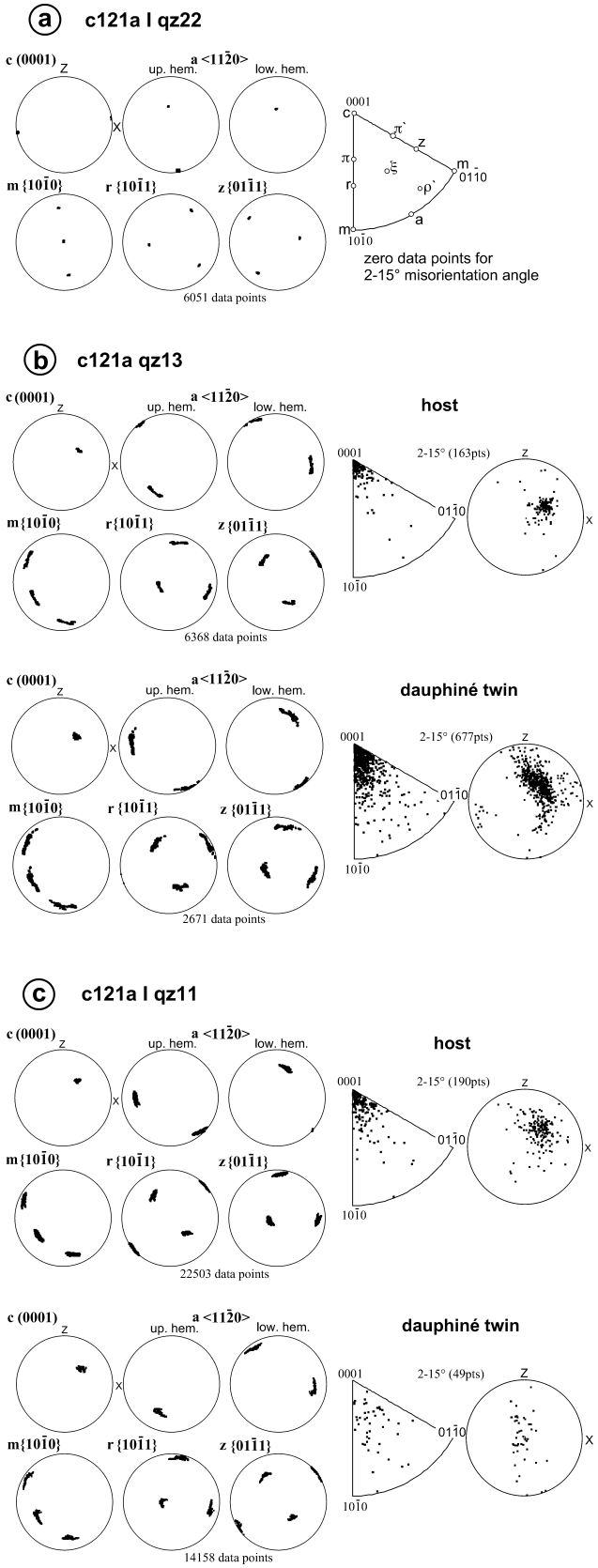

Fig. 6. (a)–(c) Orientation and misorientation data from the analysed σ-shaped quartz grains in the ultramylonite marble, related to the orientation maps presented in Fig. 4c–e: (a) scan c121a I qz22 (see Fig. 4c); (b) scan c121a qz13 (see Fig. 4d); (c) scan c121a I qz11 (see Fig. 4e). For description see Fig. 5.

The pole figure and misorientation axis plots show that, for both the host and Dauphiné orientation domains, dispersions are mainly around the crystallographic *c*-axis and to a minor extent around the poles of the π- or ξ-planes (Fig. 6).

Measured orientations of 157 individual σ-shaped quartz grains reveal a strong CPO of *c*-axis parallel to sub-parallel to the shear direction (Fig. 7b). The *a*-axes build distinct maxima in the *yz*-plane. In 20 of the measured grains, no internal deformation was visible in the OC images. The orientations of these grains are scattered across the whole range of orientation seen in the CPO (Fig. 7b).

The σ-shaped quartz grains show similar SEM-CL patterns to those of quartz grains within the protolith/protomylonite marble. Zoning patterns with facetted (e.g. Fig. 8e) and distinct SEM-CL boundaries (e.g. Fig. 8e, h and i) are still evident. But the zoning patterns are truncated with respect to the σ-shape geometry (Fig. 8e–g and i). In particular the upper right and lower left parts and sometimes the top and bottom of the cores are truncated. The wings may contain only one grey level shade (e.g. Fig. 8h and i), but also show concentric (Fig. 8e) or wedge-shaped (Fig. 8g) zoning patterns. Fig. 8j shows a multi-zoned quartz grain (grain size 100 μm) with facetted SEM-CL boundaries situated in the pressure shadow of a coarse calcite porphyroclast in the ultramylonite marble (fig. 5-10e in Bestmann, 2000). Because of the protected position in the ultramylonite, it does not show the characteristic σ-shape. All these quartz grains in the ultramylonite marble exhibit a discontinuous thin black rind (1–2 μm wide) at the interface to the surrounded calcite matrix, especially where quartz impinges adjacent calcite–calcite boundaries (see spikes in Fig. 8h).

Some horizons within the ultramylonite, parallel to the SZB, are enriched (up to 8% volume) with numerous small quartz grains (5–30 μm in diameter) interspersed within the calcite matrix (Fig. 1g). Most of the grains are individual grains surrounded by calcite. The shape of these small quartz grains is isometric to slightly elongated and never show the characteristic σ-shape. Small quartz grains have a random CPO (Fig. 7c) and show no internal distortion (Figs. 11 and 4d).

SEM-CL images reveal that the small quartz grains also show internal zoning and discontinuous dark luminescent rinds at the interface to the surrounding calcite matrix (Fig. 8f).

4.3. Summary of the observations on the quartz porphyroclasts

1. The σ-shaped quartz grains from a greenschist marble shear zone are single-crystals, sometimes twinned, but free of recrystallized grains in the wings.
2. In and out the shear zone quartz grains have the same size, though in the shear zone the σ-shaped clasts are longer according to the developed wings.

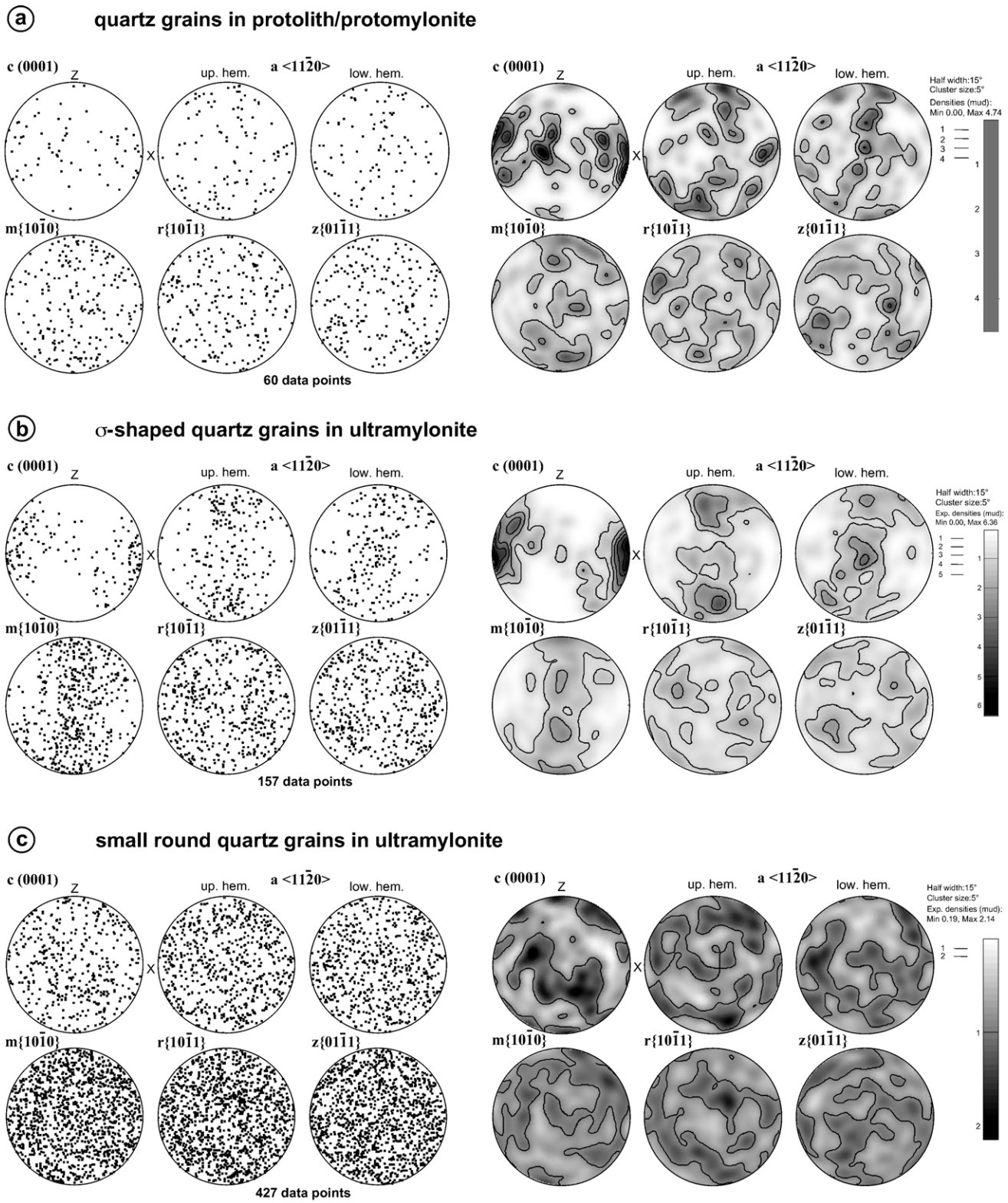

Fig. 7. Crystallographic preferred orientation (CPO) of (a) quartz grains in the protolith/protomylonite marble, (b) σ-shaped quartz grains and (c) small quartz grains (<30 μm) in the ultramylonite marble. Pole figures are equal area upper hemisphere stereoplots (see also Fig. 5). Density of contoured pole figures is given as multiple of uniform distribution (mud).

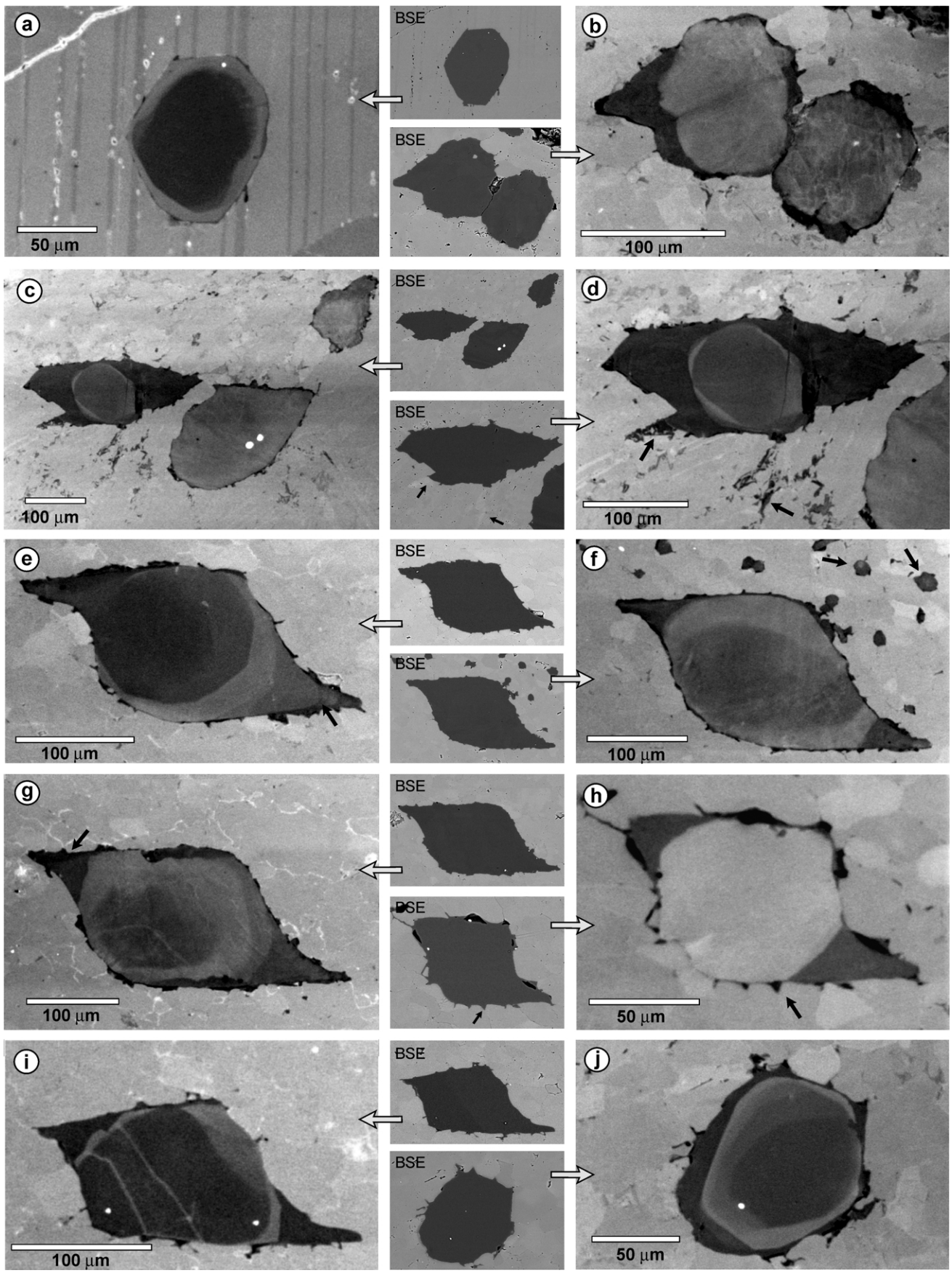
a
BSE
BSE
b
50 μm
100 μm
c
BSE
BSE
d
100 μm
100 μm
e
BSE
BSE
f
100 μm
100 μm
g
BSE
BSE
h
100 μm
50 μm
i
BSE
BSE
j
100 μm
50 μm

3. The internal deformation microstructures are the same for quartz grains in the protolith/protomylonite and ultramylonite marble (as revealed by OC images and EBSD maps).
4. The σ-shaped quartz grains show the same CL patterns as those in the protolith/protomylonite marble but are often truncated within the cores.
5. The σ-shaped quartz grains show a strong CPO with *c*-axes (sub)parallel to the shear direction.

5. Discussion

Kenkmann (2000) showed by numerical modelling that whether σ-shaped porphyroclast developed by subgrain rotation or not depends on the distribution and magnitude of the internal differential stress related to the degree of bonding between inclusion and matrix. Interface sliding favours a stress concentration within the rim of the inclusion too low for subgrain rotation. This specific rheological property might explain why the σ-shaped quartz grains are free of recrystallized grains in the wings.

However, the σ-shape of the quartz single-crystals could theoretically be explained by crystal-plasticity (i.e. dislocation creep) or by diffusive mass transfer (i.e. precipitation–dissolution creep) during strain localization in the marble shear zone. In the following section we discuss why dissolution–precipitation creep is the favourable shape-controlling deformation process (with special focus on SEM-CL patterns) rather than dislocation creep and how the measured CPO may be generated without crystal-plastic deformation.

5.1. SEM-CL patterns as evidence for dissolution–precipitation creep as shape-controlling mechanism

Since massive and pure calcite marble is relatively 'dry' and impermeable to the influx of fluids under moderate metamorphic conditions (e.g. Rye et al., 1976; Matthews et al., 1996; Bestmann, 2000) and some of the quartz grains in the protolith/protomylonite are included within coarse calcite grains (e.g. Fig. 8a), it is very unlikely that the general SEM-CL pattern, especially the zoning structures, are generated during the metamorphic history of the calcite marble. Therefore the origin of the SEM-CL patterns within individual quartz grains is more likely to be related to pre-sedimentary and/or diagenetic processes. The observed euhedral zoning around a core (Fig. 8d) is common for volcanic quartz and some plutonic rocks (Seyedolali et al., 1997; Watt et al., 1997; Götze et al., 2001). Diffuse and indistinct SEM-CL variation and even nearly uniform SEM-CL intensity (Fig. 8c) might suggest a metamorphic origin of some quartz grains (Seyedolali et al., 1997). Some of the features with weak luminescence intensity (Fig. 8d) are probably related to secondary overgrowth during diagenesis (e.g. Houseknecht, 1987).

The similarity between SEM-CL patterns in the cores of σ-shaped quartz grains and quartz grains in the protolith/protomylonite marble suggests that the cores of asymmetrical quartz porphyroclast in the ultramylonite are inherited precursor grains. This hypothesis is also supported by a multi-zoned quartz grain that does not show the characteristic σ-shape (Fig. 8j) because of its specific position in the pressure shadow of a coarse calcite porphyroclast in the ultramylonite marble.

The truncation of inherited CL zoning patterns in the cores of σ-shaped porphyroclasts gives strong evidence for diffusional mass transfer during mylonitisation (see also Walton et al., 1964; Wintsch and Knipe, 1983; Wintsch and Yi, 2002). The existence of sharp SEM-CL boundaries suggests that volume diffusion has not occurred within quartz clasts otherwise diffuse contacts between different SEM-CL zones would be expected. In particular, if volume diffusion was active during wing formation, it would have destroyed the CL patterns of the relict cores of the σ-shaped porphyroclasts. Based on the deformation mechanism map for quartz (fig. 9 in Rutter, 1976) volume diffusion in quartz

Fig. 8. SEM-CL images and corresponding backscattered (BSE) images (middle column) of quartz grains from (a)–(d) the protolith/protomylonite marble and (e)–(j) the ultramylonite marble. (a) Euhedral shaped quartz grain with SEM-CL zoning situated within a coarse calcite grain from a protolith marble. Note discontinuous thin black rind at the interface with the calcite matrix. Other quartz grains in similar microstructural positions might show a more pronounced non-luminescent rind. Vertical grey lines reflect twin set in the calcite grain. White spots and lines in the upper left corner are related to surface damage by cracks and small holes. (b)–(d) SEM-CL images of quartz grains in protomylonite marble corresponding to microstructure c121a 2er qz-rd (Figs. 1e and 4a) and microstructure c121a 3er qz-rd (Figs. 1f and 4b). (b) Note diffuse network structure with slightly brighter SEM-CL in the core of the right quartz grain corresponds to OC pattern in Fig. 1e. (c) Individual quartz grains show different SEM-CL patterns from nearly uniform SEM-CL (middle grain) through weak zoning (right grain) to distinct zoning (left grain). (d) Magnified image of left grain from (c). Note zoned core with facetted SEM-CL boundaries surrounded by weak luminescent SEM-CL exhibiting locally straight edges adjacent to calcite. Arrows mark non-luminescent patches in the calcite, which appear in the BSE image slightly brighter. (e)–(i) σ-shaped quartz grains within the ultramylonite marble showing different internal SEM-CL patterns: (e) corresponds to microstructure c121a I qz22 (Figs. 1m and 4c); (f) to microstructure c121a qz13 (Figs. 1l and 4d); (g) to microstructure c121a I qz11 (Figs. 1m and 4e). Arrows in (e) and (g) mark weak concentric and wedge-shaped zoning patterns, respectively. Arrows in (f) mark zoning patterns in small quartz grains. Quartz grain in (h) shows well-developed spikes (arrow) of quartz material penetrating into the surrounding calcite boundary network. (j) Multi-zoned quartz grain with facetted SEM-CL boundaries situated in the pressure shadow of a coarse calcite porphyroclast in the ultramylonite marble (note it does not show the characteristic σ-shape). Note all quartz grains show a more or less strongly developed non-luminescent rind at the interface to the calcite matrix. Quartz microstructures ((b)–(g)) do not correspond 100% to the respective OC images (Fig. 1e, f and k–m) because after EBSD analyses the surface had to be re-polished due to lattice damage caused by the electron beam. White spots in the SEM-CL and BSE images are related to apatite inclusions.

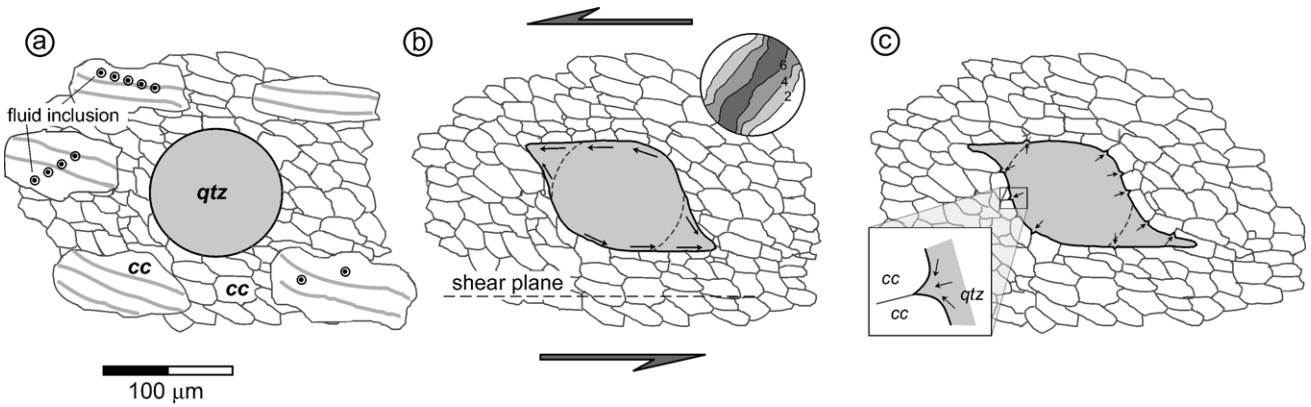

Fig. 9. Conceptual model for the formation of the σ-shaped quartz grains during shear localization within the calcite marble shear zone. (a) Spherical quartz grain (*qtz*) embedded in a protomylonitic calcite matrix (*cc*), which contains small dynamical recrystallized grains and coarse-grained porphyroclasts. Some of the coarse calcite porphyroclasts contain fluid inclusions. (b) Change of shape by dissolution–precipitation creep along interphase boundaries with respect to the flow-induced differential stress distribution (modelled by Kenkmann, 2000, fig. 9d; modelling parameter: interface sliding, gap opening; contouring represent multiple stress magnitude with respect to the average matrix stress). Arrows indicate possible diffusion pathways in quartz. (c) Quartz penetration by fine scale diffusion into surrounded calcite–calcite grain boundaries (dihedral angle) as a process to reduce internal free strain energy. Dashed line in the core of the quartz porphyroclast represents original grain.

requires much higher activation temperatures than those constrained for the greenschist marble shear zone.

The temperatures are also too low for solid-state grain boundary diffusivity (Coble creep). Instead, fluid-assisted diffusion creep, i.e. dissolution–precipitation creep (pressure solution), along interphase boundaries could explain the σ-shape of the quartz grains with its internal CL patterns. Bestmann (2000) concluded from stable isotope data that an infiltration of an external fluid into the marble shear zone is not evident. However, a small amount of fluid could be released from fluid inclusions, observed in the coarse calcite grains in the protolith/protomylonite marble (Bestmann, 2000), during dynamic recrystallization of the calcite matrix (Fig. 9a). Farver and Yund (2000) concluded from experimental data that grain boundary diffusion is enhanced in quartz in the presence of a thin fluid film along boundaries. Therefore, dissolution–precipitation creep should be able to act as a shape-controlling process for the σ-shaped quartz grains in the pressure-solution field of the deformation mechanism map (fig. 9 in Rutter, 1976) at the given temperature of 300–350 °C within the marble shear zone (see also den Brok, 1992).

Theoretically the CL truncation patterns could be explained by removal of material from the detrital precursor quartz grains by dissolution without successive precipitation (see also Wintsch and Knipe, 1983). In other words the asymmetrical quartz grains were shaped from larger precursor grains. This hypothesis would imply that the protolith/protomylonite quartz grains should be, on average, the same size or larger than the σ-shaped quartz grains (including wings). However, the grain parameter data (Fig. 2) show that the cores of σ-shaped grains in the ultramylonite are statistically the same size as the long axes of those in the protomylonite and long axes including wings are considerably larger.

Therefore, the σ-shape of the quartz grains was most likely developed by selective dissolution and subsequent precipitation. This process was also suggested to be the main mechanism causing the monoclinic shape symmetry of garnet (Azor et al., 1997), tourmaline (ten Grotenhuis et al., 2003) and sillimanite (Pennacchioni et al., 2001) developed as single-crystals in mylonitic rocks. The asymmetrical CL patterns with truncation of the core and sometimes zoned wings (e.g. Fig. 8e and g) give evidence for dissolution at interphase boundaries at high surface normal stress and syntaxial precipitation at boundaries at relatively low surface normal stress (Rutter, 1983; Lehner, 1990; Wintsch and Yi, 2002) induced by the flow pattern of the surrounding calcite matrix (Fig. 9b). However, since wings of some σ-shaped grains contain only one grey level shade, but apparently more than one zone with different SEM-CL intensity was removed (Fig. 8i), a coupled process of mass transfer along interphase boundaries and mass removal, at least for individual grains, is favoured.

The dark luminescent rind observed for all quartz grains at the interface to the calcite matrix (Fig. 8) and locally within the calcite matrix (Fig. 8d) might give evidence that some chemical exchange has occurred by diffusion between calcite matrix and quartz grains.

5.2. Why is crystal plasticity (dislocation creep) unlikely as shape-controlling mechanism?

Lattice deformation (i.e. undulose extinction, gradual lattice banding and subgrain boundaries) occurred both in quartz grains from the protolith/protomylonite and in σ-shaped quartz porphyroclasts from the ultramylonite marble as revealed by optical microscopy, OC-images and EBSD analyses (Figs. 1e and f and 4a and b). If intracrystalline deformation by slip of dislocations is assumed to have taken place, then (i) prism $\langle a \rangle$ slip is expected to have been dominant on the basis of misorientation axis analysis (Figs.

5 and 6; see also Neumann, 2000), but (ii) basal ⟨*a*⟩ slip is expected to have been dominant on the basis of the low temperature conditions (Lister and Hobbs, 1980; Price, 1985), and (iii) prism ⟨*c*⟩ slip is expected to have been dominant on the basis of the CPO pattern (Fig. 7b). This is not possible. Since prism ⟨*a*⟩slip is expected to be dominant at medium temperatures (Wilson, 1975; Lister and Dornsiepen, 1982; Law, 1990), which occurred during the pre-shear zone deformation history, the crystal-plastic deformation patterns in the σ-shaped quartz are probably inherited features. Weak intracrystalline deformation features in the wings of σ-shaped quartz grains may reflect some ongoing syn-kinematic crystal-plastic deformation during mylonitisation. However, neither the σ-shape of the quartz grains with its fixed shape orientation with respect to the specimen reference system (Figs. 1n and o), nor the CPO development can be explained by the activity of prism ⟨*a*⟩ slip. Theoretically, progressive dislocation glide using prism ⟨*c*⟩ could explain the σ-shape of those quartz grains, which reflect the main orientation component of the CPO, but not all the other σ-shaped grains that deviate from that specific crystal orientation. Furthermore, none of the internal deformation features can be related to prism ⟨*c*⟩ slip. This specific CPO pattern and inferred prism ⟨*c*⟩ slip system have only been reported from high temperature quartzitic rocks (Lister, 1981; O'Hara and Gromet, 1985; Blumenfeld et al., 1986), but never from greenschist facies rocks.

5.3. Development of shape preferred orientation (SPO) and crystal preferred orientation (CPO)

Only quartz grains with a grain size larger than the average grain size of the surrounding dynamically recrystallized calcite matrix show the characteristic asymmetrical shape and a strong SPO and CPO. All the other smaller quartz grains (<50 μm) in the ultramylonite marble have a random CPO (Fig. 7c). The uncommon CPO for quartz under greenschist facies condition with *c*-axes parallel to the shear direction can be explained by a strengthening of the weak CPO of the quartz grains present in the protolith/protomylonite marble.

Since CPO development with *c*-axis sub(parallel) to the shear direction by dislocation creep is very unlikely (see above), the following mechanisms are discussed: (1) crystallographic dependent growth and dissolution of quartz grains (Hippertt, 1994); (2) mechanic rotation of elongated quartz grains during deformation (Stallard and Shelley, 1995).

As the cores of σ-shaped quartz grains show the same CL patterns as in the protolith/protomylonite marble, crystallographic preferred growth of grains by precipitation can be excluded. If we assume that some orientations dissolve faster than others, then the ones with *c*-axes orientated at a high angle to foliation should show more flattening of the cores (see also Hippertt, 1994), which is not the case.

The shape preferred orientation of elongated cores of the σ-shaped quartz grains (Fig. 2b) is in good accordance with numerical and experimental work and observations in other natural mylonites. Elongated particles stabilise during mechanic particle rotation with their long axis subparallel (often with a low antithetic angle) to the shear direction (e.g. Jeffery, 1922; Ghosh and Ramberg, 1976; Pennacchioni et al., 2001), especially when slip occurred at the particle–matrix interface and micro shear zones developed along the top and bottom of the porphyroclast (ten Grotenhuis et al., 2002, 2003; Mancktelow et al., 2002). The asymmetric CL truncation patterns verify this hypothesis, because only a stable position ensures significant dissolution in the shortening and subsequent precipitation in the extensional quadrants of the flow during progressive strain accommodation in the calcite matrix, and thereby enhancing the characteristic σ-shape (see also ten Grotenhuis et al., 2003).

However, if we assume that the CPO pattern developed due to passive rotation of precursor clasts than the long axes should be (sub)parallel to the *c*-axis (see also Stallard and Shelley, 1995). EBSD measurements of elongated quartz grains extracted from the protolith/protomylonite marble reveal that the *c*-axes can scatter with a relatively high angle with respect to the long axis of elongated grains (Fig. 3). Even if there is a weak accordance between shape elongation and *c*-axis direction it is difficult to explain the observed CPO only by passive rotation of precursor grains, especially since all of the quartz grains in the protolith/protomylonite quartz grains have relatively low axial ratios of $R < 3$ (see also Mancktelow et al., 2002). However, many of the long axes of the cores of the σ-shaped grains are now (sub)parallel to the *c*-axis.

6. Conclusions

σ-shaped quartz grains embedded as single-crystals within a calcite matrix of a greenschist facies marble shear zone have been studied with the following conclusions:

1. Only quartz grains with a grain size larger than the average grain size of the surrounding dynamically recrystallized calcite matrix show the characteristic asymmetrical shape in the ultramylonite marble.
2. Cathodoluminescence images in the scanning electron microscope (SEM-CL) give evidence that stress-induced dissolution–precipitation creep is the favourable process providing a nearly distortion free change of shape of the quartz grains. Truncation of inherited SEM-CL patterns in the cores of the σ-shaped porphyroclasts support the hypothesis of removal of material at interphase boundaries at high surface normal stress and syntaxial accretion of wings at boundaries at relatively low surface normal stress induced by the flow pattern of the surrounding

calcite matrix. The necessary fluids may have been released from fluid inclusions during dynamic recrystallization of the calcite matrix.

3. Lattice distortion patterns (i.e. undulose extinction and subgrain boundary) in both quartz grain fractions from the protolith/protomylonite and ultramylonite marble, give evidence about the activity of dislocations during some stage of deformation. However, the development of σ-shape is not related to the crystallographic orientation of the quartz porphyroclasts. Crystallographic misorientation analysis by electron backscatter diffraction (EBSD) technique analysis revealed that crystal-plastic deformation is unlikely to be the main mechanism responsible for the development of the σ-shape of quartz grains.
4. The σ-shaped quartz grains have a strong CPO, with *c*-axes (sub)parallel to the shear direction. This fabric is uncommon for quartz under greenschist facies conditions. It can be explained by a strengthening of a pre-existing weak CPO during mylonitisation. Since the quartz grains are not elongated accurately parallel to the *c*-axis rigid particle, rotation alone cannot explain the development of the CPO.

Acknowledgements

We thank Karsten Kunze, John Wheeler and Norio Shigematsu for stimulating discussions. The manuscript was much improved by the reviews of Bas den Brok and Giorgio Pennacchioni. Michel Bestmann kindly acknowledges financial support by the Graduiertenförderungsprogramm (Bayern) and the Deutsche Forschungsgemeinschaft (DFG-grant BE 2413/1-1). The CamScan X500 was funded by HEFCE through grant JR98LIPR. SEM consumables were funded by NERC grants GR3/11475 and NER/A/5/2001/01181. Final revision of the manuscript was done and funded by FWF project 15668 in Vienna, Austria. Further images of σ-shaped quartz grains are available from http://www.geol.uni-erlangen.de/michel.

References

Adams, B.L., Wright, S.I., Kunze, K., 1993. Orientation imaging: the emergence of a new microscopy. Metallurgical Transactions 24A, 819–831.

Azor, A., Simancas, J.F., Exposito, I., Gonzales Lodeiro, F., Martinez Poyatos, D.J., 1997. Deformation of garnets in a low-grade shear zone. Journal of Structural Geology 19, 1137–1148.

Bestmann, M., 2000. Evolution of a shear zone in calcite marble on Thassos Island, Northern Greece: results from microfabrics and stable isotopes. Erlanger Geologische Abhandlungen 131, 1–127.

Bestmann, M., Prior, D.J., 2003. Intragranular dynamic recrystallization in naturally deformed calcite marble: diffusion accommodated grain boundary sliding as a result of subgrain rotation recrystallization. Journal of Structural Geology 25, 1597–1613.

Bestmann, M., Kunze, K., Matthews, A., 2000. Evolution of a calcite marble shear zone complex on Thassos Island, Greece: microstructural and textural fabrics and their kinematic significance. Journal of Structural Geology 22, 1789–1807.

Blumenfeld, P., Mainprice, D., Bouchez, J.-L., 1986. C-slip in quartz from subsolidus deformed granite. Tectonophysics 127, 97–115.

Dell'Angelo, L.N., Tullis, J., 1989. Fabric development in experimentally sheared quartzites. Tectonophysics 169, 1–21.

den Brok, S.W.J., 1992. An experimental investigation into the effects of water on the flow of quartzite. Geologica Ultrajectina 95, 1–178.

Dinter, D.A., 1998. Late Cenozoic extension of the Alpine collisional orogen, north-eastern Greece: origin of the north Aegean basin. Geological Society of America Bulletin 110, 1208–1230.

Farver, J., Yund, R., 2000. Silicon diffusion in a natural quartz aggregate: constraints on solution-transfer diffusion creep. Tectonophysics 325, 193–205.

Fynn, G.W., Powell, W.J.A., 1979. The Cutting and Polishing of Electro-optic Materials. Adams Hilger, London.

Ghosh, S.K., Ramberg, H., 1976. Reorientation of inclusions by combination of pure shear and simple shear. Tectonophysics 34, 1–70.

Götze, J., Plötze, M., Habermann, D., 2001. Origin, spectral characteristics and practical applications of the cathodoluminescence (CL) of quartz—a review. Mineralogy and Petrology 71, 225–250.

Hippertt, J.F. 1994. Microstructures and *c*-axis fabrics indicative of quartz dissolution in sheared quartzites and phyllonites. Tectonophysics 229, 141–163.

Houseknecht, D.W., 1987. Assessing the relative importance of compaction processes and cementation to reduction of porosity in sandstones. American Association of Petroleum Geologists Bulletin 71, 633–642.

Jeffery, G.B., 1922. The motion of ellipsoidal particles immersed in a viscous fluid. Proceedings of the Royal Society of London, Series A 102, 161–179.

Kenkmann, T., 2000. Processes controlling the shrinkage of porphyroclasts in gabbroic shear zones. Journal of Structural Geology 22, 471–487.

Law, R.D., 1990. Crystallographic fabrics: a selective review of their application to research in structural geology. In: Knipe, R.J., Rutter, E.H. (Eds.), Deformation Mechanisms, Rheology and Tectonics. Geological Society Special Publications 54, pp. 335–352.

Lehner, F.K., 1990. Thermodynamics of rock deformation by pressure solution. In: Barber, D.J., Meredith, P.D. (Eds.), Deformation Processes in Minerals, Ceramics and Rocks, Unwin Hyman, London, pp. 296–333.

Lister, G.S., 1981. The effect of the basal-prism mechanism switch on fabric development during plastic deformation of quartzite. Journal of Structural Geology 3, 67–75.

Lister, G.S., Dornsiepen, U.F., 1982. Fabric transition in the Saxony granulite terrain. Journal of Structural Geology 41, 81–92.

Lister, G.S., Hobbs, B.E., 1980. The simulation of fabric development during plastic deformation and its application to quartzites: the influence of deformation history. Journal of Structural Geology 2, 255–370.

Lloyd, G.E., 1987. Atomic number and crystallographic contrast images with the SEM: a review of backscatter techniques. Mineralogical Magazine 51, 3–19.

Mancktelow, N.S., Arbaret, L., Pennacchioni, G., 2002. Experimental observations on the effect of interface slip on rotation and stabilisation of rigid particles in simple shear and a comparison with natural mylonites. Journal of Structural 24, 567–585.

Matthews, A., Liati, A., Mposkos, E., Skarpelis, N., 1996. Oxygen isotope geochemistry of the Rhodope polymetamorphic terrain in northern Greece: evidence for the preservation of pre-metamorphic isotopic compositions. European Journal of Mineralogy 8, 1139–1152.

Neumann, B., 2000. Texture development of recrystallised quartz polycrystals unravelled by orientation and misorientation characteristics. Journal of Structural Geology 22, 1695–1711.

O'Hara, K., Gromet, L.P., 1985. Two distinct Precambrian (Avalonian) terranes in southeastern New England and their late Paleozoic juxtaposition. American Journal of Sciences 285, 673–709.

Passchier, C.W., Simpson, C., 1986. Porphyroclast systems as kinematic indicators. Journal of Structural Geology 8, 831–843.

Passchier, C.W., Sokoutis, D., 1993. Experimental modelling of mantled porphyroclasts. Journal of Structural Geology 15, 895–910.

Pennacchioni, G., Di Toro, G., Mancktelow, N.S., 2001. Strain-insensitive preferred orientation of porphyroclasts in Mont Mary mylonites. Journal of Structural Geology 23, 1281–1298.

Peterek, A., Polte, M., Wölfl, C., Bestmann, M., Lemtis, O., 1994. Zur jungtertiären geologischen Entwicklung im SW der Insel Thassos (S-Rhodope, Nordgriechenland). Erlanger geologische Abhandlungen 124, 29–59.

Price, G.P., 1985. Preferred orientation in quartzites. In: Wenk, H.R., (Ed.), Preferred Orientation in Deformed Metals and Rocks: an Introduction to Modern Texture Analysis, Academic Press, Orlando, pp. 385–406.

Prior, D.J., 1999. Problems in determining the misorientation axes, for small angular misorientations, using electron backscatter diffraction in the SEM. Journal of Microscopy 195, 217–225.

Prior, D.J., Trimby, P.W., Weber, U.D., Dingley, D.J., 1996. Orientation contrast imaging of microstructures in rocks using forescatter detectors in the scanning electron microscope. Mineralogical Magazine 60, 859–869.

Prior, D.J., Wheeler, J., Peruzzo, L., Spiess, R., Storey, C., 2002. Some garnet microstructures: an illustration of the potential of orientation maps and misorientation analysis in microstructural studies. Journal of Structural Geology 24, 999–1011.

Rutter, E.H., 1976. The kinetics of rock deformation by pressure-solution. Philosophical Transactions of the Royal Society of London A 283, 203–219.

Rutter, E.H., 1983. Pressure solution in nature, theory and experiment. Journal of Geological Society of London 140, 725–740.

Rye, R.O., Schuiling, R.D., Rye, D.M., Jansen, J.B.H., 1976. Carbon, hydrogen, and oxygen isotope studies of the regional metamorphic complex at Naxos, Greece. Geochimica et Cosmochimica Acta 40, 1031–1049.

Seyedolali, A., Krinsley, D.H., Boggs, S., O'Hara, P.F., Dypvik, H., Goles, G.G., 1997. Provenance interpretation of quartz by scanning electron microscope-cathodoluminescence fabric analysis. Geology 25, 787–790.

Stallard, A., Shelley, D., 1995. Quartz c-axes parallel to stretching direction in very low-grade metamorphic rocks. Tectonophysics 249, 31–40.

ten Grotenhuis, S.M., Passchier, C.W., Bons, P.D., 2002. The influence of strain localisation on the rotational behaviour of rigid objects in experimental shear zones. Journal of Structural Geology 24, 485–499.

ten Grotenhuis, S.M., Trouw, R.A.J., Passchier, C.W., 2003. Evolution of mica fish in mylonitic rocks. Tectonophysics 372, 1–21.

Tullis, J., Yund, R.A., 1985. Dynamic recrystallization of feldspar: a mechanism of ductile shear zone formation. Geology 13, 238–241.

Walton, M., Mills, A., Hansen, E., 1964. Compositionally zoned granitic pebbles in three metamorphosed conglomerates. American Journal of Science 262, 1–25.

Watt, G.R., Wright, P., Galloway, S., McLean, C., 1997. Cathodoluminescence and trace element zoning in quartz phenocrysts and xenocrysts. Geochimica et Cosmochimica Acta 61, 4337–4348.

Wawrzenitz, N., Krohe, A., 1998. Exhumation and doming of the Thasos metamorphic core complex (S Rhodope, Greece): structural and geochronological constraints. Tectonophysics 285, 301–332.

Wheeler, J., Prior, D.J., Jiang, Z., Spiess, R., Trimby, P.J., 2001. The petrological significance of misorientations between grains. Contributions to Mineralogy and Petrology 141, 109–124.

Wilson, C.J.L., 1975. Preferred orientation in quartz ribbon mylonites. Bulletin Geological Society of America 86, 968–974.

Wintsch, R.P., Knipe, R.J., 1983. Growth of a zoned plagioclase porphyroblast in a mylonite. Geology 11, 360–363.

Wintsch, R.P., Yi, K., 2002. Dissolution and replacement creep: a significant deformation mechanism in mid-crustal rocks. Journal of Structural Geology 24, 1179–1193.